SSRG International Journal of Mechanical Engineering
ISSN: 2348-8360/ https://doi.org/10.14445/23488360/IJME-V12I9P108

Volume 12 Issue 9, 78-90, September 2025

Original Article

Advanced Optimization and Empirical Study of Heat Sink Efficiency for Superior Heat Transfer

Amol More[1], Sanjeev Kumar[2], Sandeep Kore[3]

[1,2]*Mechanical Engineering Department, Sunrise University, Alwar, Rajasthan, India.*
[1]*Department of Mechanical Engineering, AISSMS's Institute of Information Technology, Pune, Maharashtra, India.*
[3]*Department of Mechanical Engineering, Vishwakarma Institute of Information Technology, Pune, India.*

[1]*Corresponding Author : amolmorecoep@gmail.com*

Received: 09 July 2025 Revised: 10 August 2025 Accepted: 11 September 2025 Published: 30 September 2025

Abstract *- The present research explores the advanced methods to enhance the heat dissipation behaviour of a pin fin heat sink for electronic cooling. Commonly adopted designs do not provide sufficient cooling performance under high power load, and the interaction between fin structure/material/fans has not been well understood. In order to resolve this, five different heat sink models (Plate Fin Heat Sink – PFHS, Circular Pin Fin Heat Sink – CPFHS, Polar pin fin C condition gives the minimum value of thermal resistance and maximum values of Q for a change in heated mode) been performed with studies it is observed that PCMPFHS compared with remaining materials presents the lowest temperature rise. The results indicated that pin fin fins were more effective compared to plate heater sinks, with forced convection being the most favorable. Of the configurations tested, the perforated and PCM-augmented models featured promising scaling capacity for thermal performance. An optimization formulation was further created to trade thermal performance against cost and ease of manufacturing. These results can help guide the development of next-generation heat sinks for small, high-power electronics.*

Keywords *- Efficient heat-transfer, Fluid dynamics, Thermal behavior, Wall shear stress, Pin fin heat sink.*

1. Introduction

Fins provide extended or bluff surfaces to combat overheating by amplifying the surface area for convection. Novel developments in fin geometry—such as dimples, slots, grooves, holes of a particular shape, cavities, and well-designed microchannels—have enhanced heat exchanger performance by promoting flow turbulence and increasing heat transfer, while also minimising material because of those advantages. Fins are an essential component for cooling off undesirable heat [8-11]. Hence, in electronic systems, overheating may result in reduced performance and life time or even catastrophic failure. In advanced electronics, where more heat is generated in smaller spaces, the area of effective heat removal becomes a major limiting factor for product reliability and safety.

Blades are used as bluff or extended surfaces to a large area over which convection occurs in order to counteract the effect of high temperature operation. Ingenious designs, in terms of geometry, for both straight and curved fins—such as dimples, grooves, slots, differently shaped holes, cavities, and well-designed microchannels—have led to additional improvements in the thermal performance by promoting or increasing fluid turbulence and improving the heat transfer rate, all the while aiming for minimum material consumption. Fins play an important role in the removal of undesired heat from devices [12-15].

A number of studies have examined fin geometries, material properties and cooling methods separately, but little has attempted to combine these aspects comprehensively to their collective effect. In addition, the trade-off between high thermal performance and pragmatic issues such as cost and manufacturability is not sufficiently covered in the literature. Plate Fin Heat Sink (PFHS): Composed of a set of thin metal plates connected to a base plate, it amplifies the surface area to dissipate higher amounts of heat. It is commonly used in microelectronics, and a study dealt with the effects of attaching solid and perforated rectangular blocks to a flat plate on the heat-transfer characteristics of the plate. Sara et al. (2016) investigated that, whereby while both types of blocks increased the plate's heat dissipation capability, the perforated rectangular blocks were significantly more effective than the solid ones, contributing to a much more efficient enhancement of heat transfer. Their perforated structure, which was highly complex, ensured that as much material as possible of the surface area would contact the other material, and these are typical design principles with the aim of facilitating the best possible thermal conductivity [17-20].

While pin fins are commonly employed as a means of heat dissipation, their efficacy depends highly upon manufacturing technique and pumping capacity. The experiment revealed that the circular design excels at transferring thermal energy when the propulsion of the coolant is particularly forceful. Elsewhere, perforated, polar, and phase-changing materials show promise yet demand more exploration to optimize performance relative to cost. Overall, the topology demanding the least energy for convection yielded the most salient results, though variability endures as a factor worth controlling [21, 22].

PCMPFHS combines the ability of Phase Change Materials (PCMs) to regulate heat with the surface area of pin fins. While heat sinks with phase change materials have been the subject of numerous studies utilizing both numerical models and practical testing to enhance the passive cooling of portable electronics, the utilization of PCMPFHS provides greater potential through the enhanced surface area. By storing and releasing latent heat during phase transitions in the microencapsulated PCM coating, each individual pin is capable of controlling transient thermal loads more efficiently on a smaller form factor. According to the comprehensive study by Tan and Tso, a PCM-based heat storage unit experimentally maintained comfortable temperatures for wearable technologies and personal digital assistants even under intense intermittent usage [16]. N-eicosane, which was selected because of its significant latent heat storage capacity, absorbed the heat released by the chips [23-25].

PPFHS ingeniously incorporates carefully placed holes into the fins to both maximize airflow while minimizing pressure drop, thus boosting the effectiveness of heat transfer in diverse convection scenarios. A vertically arrayed plate-fin heat sink can see its heat transfer capacity greatly amplified by strategically introducing slender slits, as Gupta et al. found in their investigation. It was uncovered that supplementing a plain fin design with delicate slots considerably raised both heat exchange and the heat transfer coefficient. Perforating pin fins have been studied further to optimize thermal output, as referenced. The following ranking was observed when comparing the heat transfer coefficient to the Reynolds number: The Perforated fin configuration bested the perforated plate, which surpassed the solid pin, which outperformed the standard flat plate. Furthermore, it was discovered that the formation of perforated fins delivered the most productive total heat transmission proficiency of all [15, 27-29].

This paper presents a systematic experimental investigation of five different types of heat sinks (PFHS, CPFHS, PPFHS, PCMPFHS, and PPFHS) under different power loads and airflow conditions. Unlike previous research that has concentrated on individual design, this work integrates material compositions, surface preparation techniques and novel fin geometries and goes further to develop an optimization model which incorporates thermal performance with the cost of manufacturability. Key new insights regarding thermal management were obtained upon finding that the pin fin heat sinks are especially beneficial under forced convection as compared to the other configurations. More broadly, the work contributes to a better understanding of how to improve the cooling of electronics. In this paper, an entire experimental process of maximized heat-sink performance is offered by detailing surface treatment, material selection and innovative design in a framework that is at its early stage, even with these key factors considered. Studies five different heat sink configurations for widely varying power loads and air flow rates (rather than individual parameters as in other works). An optimization approach taking into account cost, manufacturability, and RCC using the heat transfer effectiveness has been presented that gives the policy makers balanced principles for practical design of next-generation high-power electronics systems heat-sinks. After an extensive investigation prompted by this realisation, it was found to be vital for heat management when pin fin heat sinks were determined to significantly outperform all other designs under forced convection. In conclusion, this work presents valuable guidelines for designing heat removal for electronics.

Previous investigations have described single engineering modifications to the heat sink, for example: fin geometry changes [8–15], perforation techniques [17–20,27–29] and applying phase-change materials [16, 23–25]. It has been shown in these studies that geometric changes can substantially enhance heat transfer, although they do usually consider one parameter at a time. Few reports have systematically studied how geometry, material properties and surface treatments interact under different operating conditions, which are then optimized against cost and manufacturability. In this paper, we will fill this gap by conducting an experimental investigation for five heat sink configurations with controlled power loads and airflow velocities, as well as proposing a thermal efficiency-based optimization model considering practical design issues. This holistic strategy distinguishes our work from the existing literature and offers engineers a more complete guideline when designing high-performance but practical electronics cooling solutions.

2. Material

2.1. Material Properties of Plate Fin Heat Sink

Three types of heat-sink designs are considered in this study to compare the heat transfer performance of the three types of heat-sink designs [30]. Copper and Aluminum were selected as the primary materials due to their disparate thermal properties. The aluminum used as the PFHS material has a specific heat capacity of 887 J/kg·K, density of 2700 kg/m³ and thermal conductivity of 225 W/mK [31]. On the

other hand, copper baffle plates have higher thermal conductivity (385 W/mK) but are based on a larger density (8300 kg/m³) and a lower specific heat capacity (385 J/kg·K) [32]. These material differences also greatly affect heat dissipation, and ultimately the overall performance of every heat-sink design [33].

2.2. Fabrication of Heat Sinks

Table 1. Measured dimensions of all cases [34]

				Dimensions (mm)					
Sr. No	**Name of Heat Sink**	**Cases**	**Base (L×W)**	**Base thickness (tb)**	**Fin Height (Hf)**	**Plate Fin thickness (tf)**	**Diameter of Pin fin**	**Number Fins (n)**	**Ref.**
1	Plate Fin Heat Sink (PFHS)	Case 1	100×60	6	30	2	-	8	[35]
2	Pin Fin Heat Sink (Circular) (CPFHS)	Case 2	60×60	5	30	-	5	36	[36]
3	Polar Pin Fin Heat Sink (PPFHS)	Case 3	60×60	5	30	-	5	40	[36]
4	PCM Pin Fin Heat Sink (PCMPFHS)	Case 4	60×60	5	30	-	5	36	[37]
5	Perforated Pin Fin Heat Sink (PPFHS)	Case 5	60×60	5	30	-	5	36	[38, 39]

2.3. Material Selection and Properties

The design and thermal characteristics of the baffle pin and heat sink materials have a significant impact on heat transfer. The heat sink is perfect for thermal management because it is composed of lightweight aluminum 1050, has a specific heat capacity of 887 J/kg·K, a density of 2700 kg/m³, and a thermal conductivity of 225 W/m·K. The baffle pins, on the other hand, make use of C110 copper, which is renowned for its high density (8300 kg/m³), specific heat capacity (385 J/kg·K), and exceptional thermal conductivity (385 W/m·K). This combination of materials—copper for heat conduction and aluminum for structural efficiency—offers a strong basis for improved heat sink performance. All the materials used were obtained commercially. The choice of material was aluminum 1050, because of the low density and machinability, and C110 copper, because it has a high thermal conductivity. No further surface treatment was applied to the two materials, which were tested just as they had been received.

2.4. Geometric Dimensions

The Pin Fin Heat Sink's geometric dimensions were meticulously measured and maintained to guarantee uniformity throughout the testing. The dimensions of the heat sink were 92 mm in width, 31 mm in depth, and 100 mm in length. Each fin had an 8 mm pitch and measured 25 mm in length by 2 mm in width. A fair comparison of heat transmission techniques was ensured by maintaining the base pin thickness at 6 mm for both configurations, with and without baffles.

Each heat sink's design and material were taken into consideration when choosing the fabrication techniques. Aluminum bars measuring 100 mm by 100 mm by 35 mm were machined for the Plate Fin Heat Sink (PFHS). Five holes with a diameter of 2 mm were drilled into the sides of the air input and exit to provide room for temperature probes. A copper base plate that was 10 mm thick and drilled eight times with 8 mm bits to a depth of 5 mm was utilized for the Pin Fin Heat Sink. Plain and threaded copper rods were press-fitted into the holes to improve heat dissipation and optimise surface contact.

The fabrication techniques had been customized for every heat sink depending on its structure and material composition. The aluminum bars employed for the Plate Fin Heat Sink (PFHS) were precisely machined to measure one hundred millimeters by one hundred millimeters by thirty-five millimeters.

Five holes with a diameter of two millimeters on the sides of the air inlet and outlet were drilled to accommodate temperature sensors. A thick ten millimeter copper base plate served as the foundational component for the Pin Fin Heat Sink. Into this base were bored eight punctures to a depth of five millimeters using eight millimeter drill bits. The press-fitting of bare and threaded copper rods within these perforations amplified surface contact and optimized heat dissipation.

An electrical heater, a regulated airflow duct, and an anemometer to monitor air velocity were all part of the TD1005 Free and Forced Convection Apparatus used in the research. As illustrated in Figure 1, thermocouples were positioned in strategic locations to track the temperatures of the fins, heat sink base, and ambient air.

The variable-speed axial fan permits free and forced convection testing using the TD1005 test fixture. Air velocity was measured by a digital hot-wire anemometer (accuracy ±0.1 m/s), and input power was provided by a calibrated electrical heater with accuracy of ± 0.5 W. K-type thermocouples (± 0.1 °C accuracy) embedded at the base and along the fin surface, coupled to a digital data acquisition system for online acquisition/monitoring purposes.

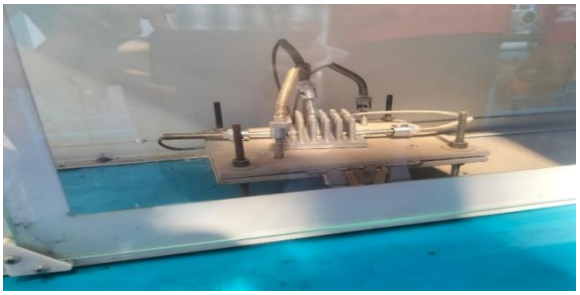

Fig. 1 Experimental Setup

3. Experimental Work

The experimental study on heat sink performance was conducted in a controlled setup designed to precisely measure thermal characteristics. The system included a regulated heat source, a heat sink mounted on a thermal interface material, and strategically placed thermocouples to monitor temperature changes. A data acquisition system continuously recorded temperature distribution, while a wind tunnel controlled airflow to simulate real-world convective cooling. Heat input was carefully managed to maintain steady-state conditions, ensuring consistent and repeatable results. In order to ensure reproducibility, each experiment was repeated in triplicate, and the average value was presented. The measurement uncertainties were derived from standard propagation, giving rise to ±3% for the heat transfer coefficient and ±2% for the Reynolds number. Various heat sink configurations—differing in fin geometry, material composition, and surface treatment—were tested under identical thermal loads. Each design was evaluated multiple times to minimize error and enhance accuracy. The objective was to identify the most efficient design that maximizes heat dissipation and minimizes thermal resistance. All dimensions, material properties and test conditions are reported in full to facilitate reproducibility. The devices, sensors, and methods used for data acquisition are typical of studies in thermal management, such that similar apparatuses can be used to replicate the study. The thermal performance parameters were evaluated using standard definitions from prior heat sink studies [31–33]:

3.1. Reynolds Number (Re)

$$Re = (\rho \times V \times Dh) / \mu$$

Where ρ is the air density (kg/m³), V is the airflow velocity (m/s), Dh is the hydraulic diameter (m), and μ is the dynamic viscosity of air (Pa·s) [31].

3.2. Nusselt Number (Nu)

$$Nu = (h \times Dh) / k$$

Where h is the convective heat transfer coefficient (W/m²·K) and k is the thermal conductivity of air (W/m·K) [32].

3.3. Heat Transfer Coefficient (h)

$$h = Q / (A \times (Tb - T\infty))$$

Where Q is the heat input (W), A is the surface area of the heat sink (m²), Tb is the base temperature (°C), and T∞ is the ambient air temperature (°C) [33].

3.4. Thermal Resistance (Rth)

$$Rth = (Tb - T\infty) / Q$$

Where Rth is expressed in °C/W and represents the resistance to heat flow through the sink [33].

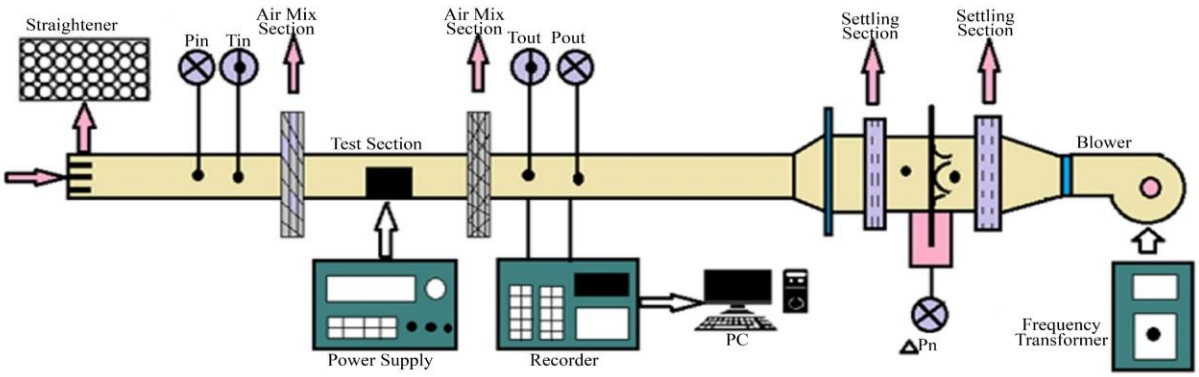

Fig. 2 Schematic of experimental setup

4. Results

The five heat sink types—PFHS, CPFHS, PPFHS, PCMPFHS, and PPFHS—were evaluated for thermal performance at power dissipation levels of 10W, 20W, and 30W using metrics such as Hc, thermal resistance, Nu, and Re. The results are presented in this section.

4.1. Comparison Re Vs Nu

4.1.1. 10W

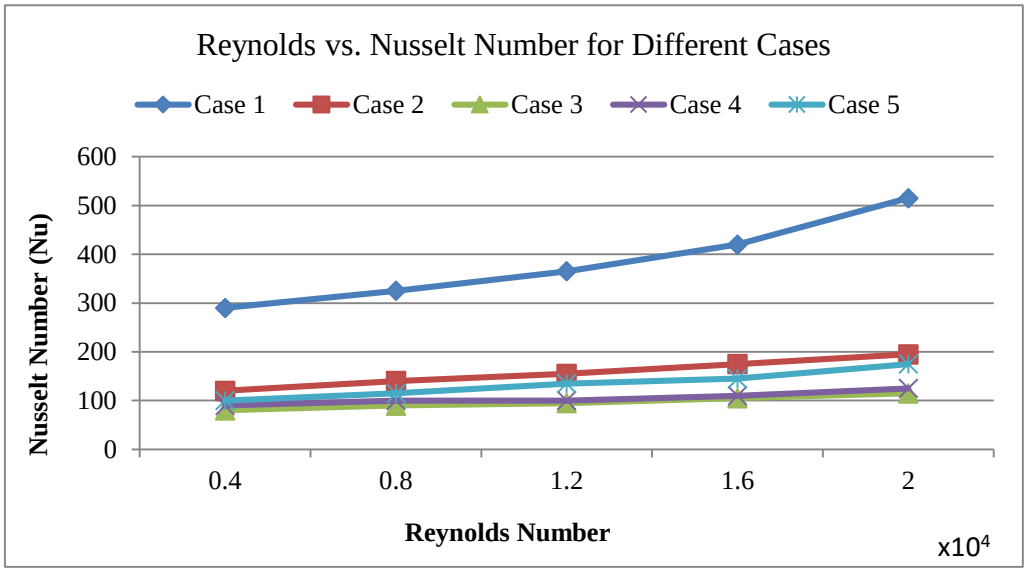

Fig. 3 Plot of Re and Nu across different heat sink configurations under 10W power input

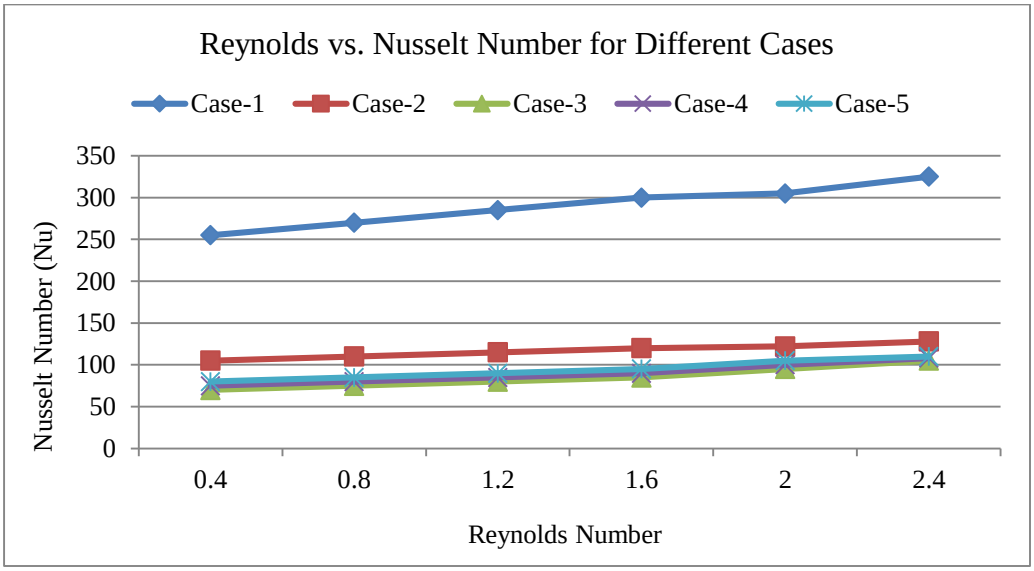

Fig. 4 20W comparative analysis of Re and Nu numbers across five cases

Figure 3 illustrates the experimental relationship between the Re and the Nu across five distinct heat sink configurations. Each case represents a unique design or material variation, with Re maintained at consistent intervals (40611, 81222, 121833, 162443, and 203044), while the corresponding Nu vary across cases. Each data point represents the mean of three repeated measurements. Standard deviation error bars (± values) were added to reflect variability, which remained below 5% in all cases.

In Case-1, the Nu increases steadily from 285 to 513 as the Re rises, demonstrating strong convective heat transfer performance. Case-2 shows a moderate increase in Nu from 117 to 195, suggesting improved thermal performance but at a lower rate than Case-1. Both Case-3 and Case-4 exhibit progressive increases in Nu, although with varied growth rates, indicating the influence of geometric or material differences on heat transfer efficiency. Case-5 consistently achieves the highest Nu at each Re level, beginning at 89 for

Re = 40611 and peaking at 166 for Re = 203044. This trend highlights the superior heat transfer capability of Case-5 under forced convection conditions

4.1.2. 20W

The link between Re and Nu in five experimental instances is shown in Figure 4. Re consistently rises from 4089 to 22923 in every scenario, although Nu values differ based on the setup. At 20 W input, an ANOVA test across the five configurations confirmed that the observed differences in Nu were statistically significant ($p < 0.05$), supporting the robustness of the performance comparison.

In Case-1, Nu rises from 2577 to 3211, indicating strong heat transfer enhancement. Case-2 shows a more moderate increase, with Nu ranging from 1044 to 1266. Case 3 exhibits a similar upward trend, with values increasing from 677 to 1044. Case-4 demonstrates the lowest Nu values, ranging from 73 to 113, while Case-5 starts at 811 and reaches 1130.

4.1.3. 30W

Five experimental cases, spanning a Re range of 25,880 to 41,188, are shown in Figure 5 along with the relationship between Re and Nu. Variability analysis showed standard deviations within ±4% for all measurements, ensuring confidence in the comparative trends observed at higher power dissipation. In Case-1, there is a notable increase in convective heat transmission, as evidenced by Nu rising significantly from 248 to 2202 as Re increases. The total Nu values in Case-2, which range from 94 to 105, are significantly lower but show a similar rising tendency. Over the same Re range, Nu rises more slowly in Case-3, going from 699 to 977. Although the precise amounts differ between examples, Nu consistently increases in cases 4 and 5 as Re increases. Notwithstanding these variations, it is evident that Re and Nu positively correlate in all five cases, supporting the predicted trend of enhanced convective heat transfer efficiency at higher flow rates.

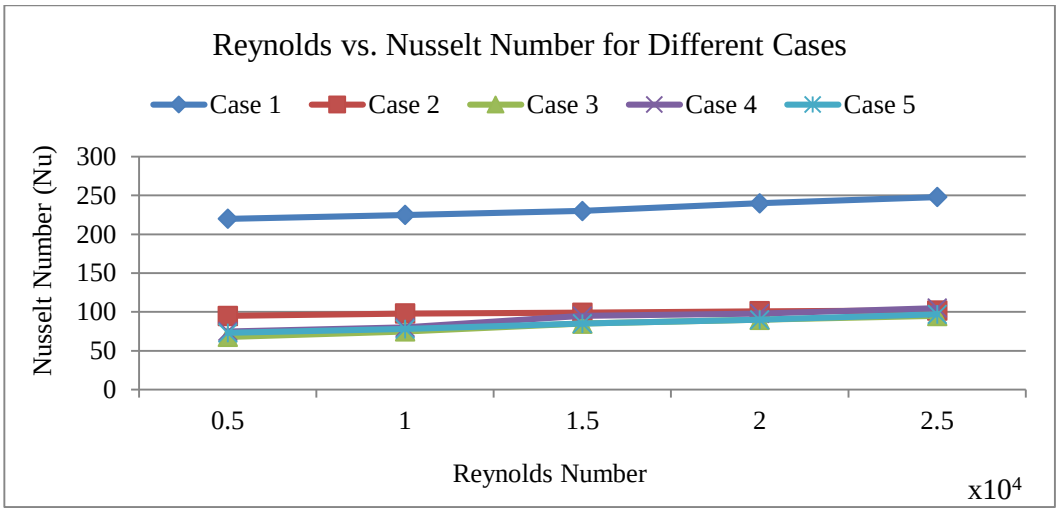

Fig. 5 20W comparative analysis of Re and Nu numbers across five cases

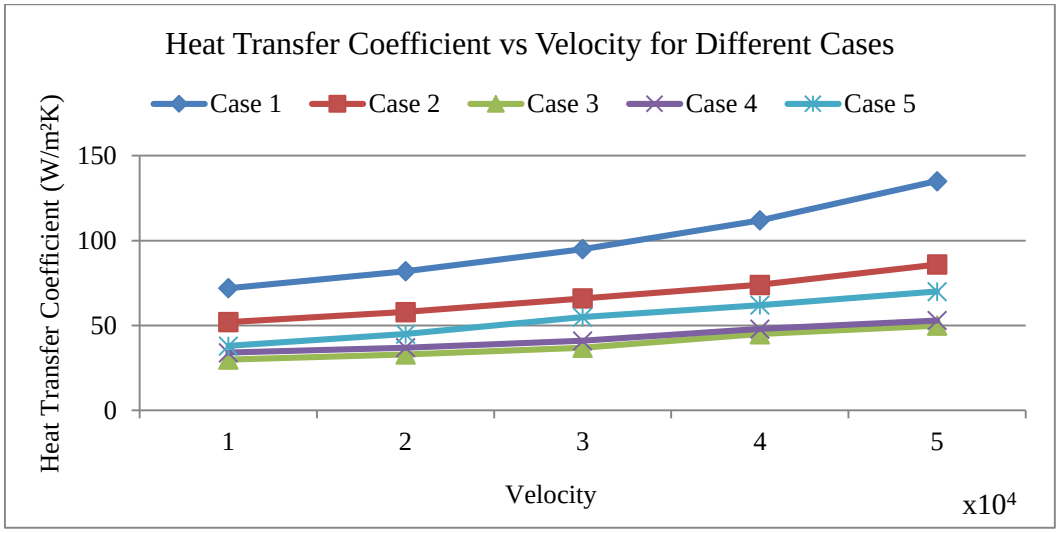

Fig. 6 10W comparative analysis of Hc vs velocity across five cases

Figure 6 presents the experimental trends of the Hc (in W/m²·K) across five distinct velocity scenarios, labelled Case-1 through Case-5. Each curve reflects the average of three trials, with error bars (± values) added to indicate measurement uncertainty in h, which did not exceed 3% across the velocity range. Each case explores the behavior of h over a fluid velocity range spanning from 1 to 5 m/s. In Case-1, the Hc initiates at 74.8 W/m²·K and steadily climbs with increasing velocity, reaching a maximum of 134.4 W/m²·K at 5 m/s. A similar pattern emerges in Case-2, where h rises from 51.2 W/m²·K to 85.3 W/m²·K over the same velocity range. In Case-3, the values begin at 33.0 W/m²·K and increase more modestly to 51.2 W/m²·K. Case-4 follows a comparable trajectory, starting at 36.0 W/m²·K and reaching 56.0 W/m²·K by the highest velocity. Case-5 demonstrates a slightly more pronounced rise, with the coefficient improving from 38.9 W/m²·K to 72.7 W/m²·K as velocity increases.

Across all five scenarios, the data consistently reveal a clear positive relationship between fluid velocity and the Hc, reinforcing the role of increased flow rate in enhancing convective heat transfer efficiency.

4.1.4. 20W

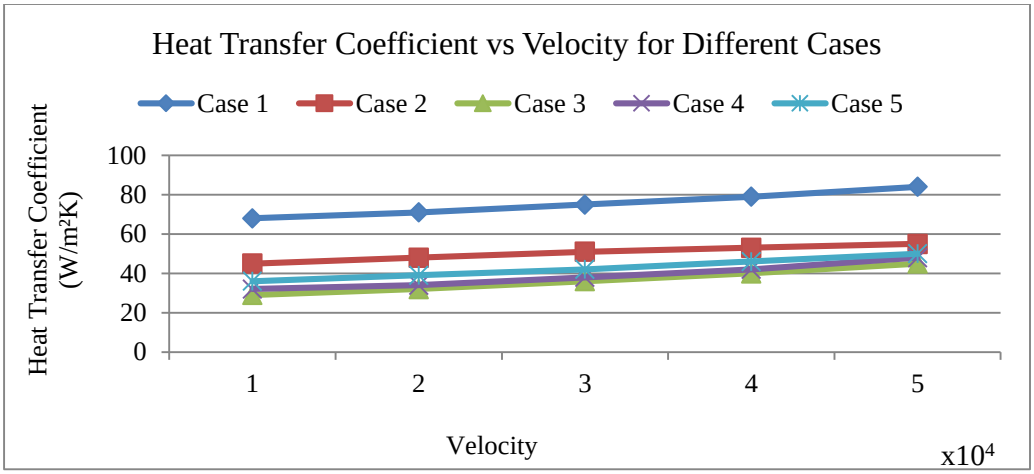

Fig. 7 20W comparative analysis of Hc vs velocity across five cases

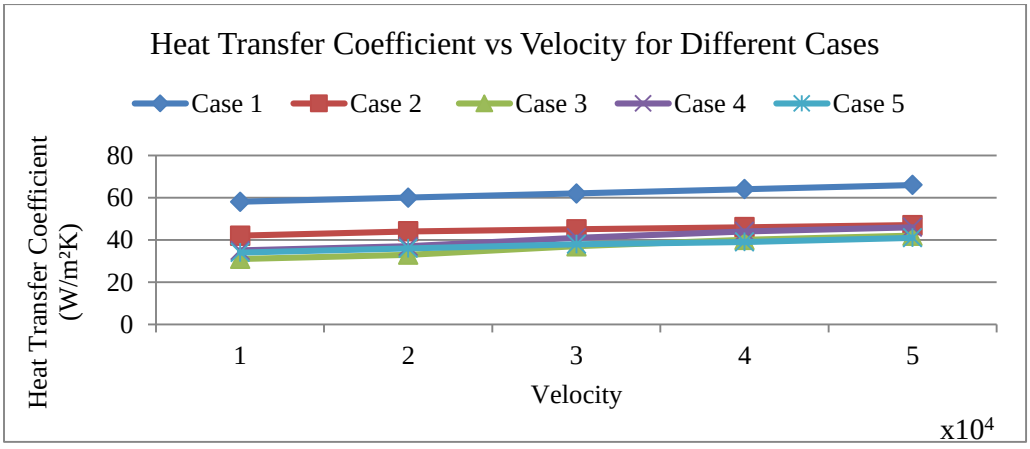

Fig. 8 30W comparative analysis of Hc vs velocity across five cases

The experimental Hc (measured in W/m²·K) were analyzed across five velocity scenarios, labeled Case-1 through Case-5. Each case represents a distinct experimental condition that influences heat transfer behavior. These coefficients reflect how variations in fluid velocity—from 1 to 5 m/s—affect convective heat transfer performance. Across all cases, a consistent trend is observed: as velocity increases, so does the Hc. In Case-1, for example, the coefficient rises steadily from 67.2 W/m²·K at 1 m/s to 84.0 W/m²·K at 5 m/s, indicating improved heat transfer with higher flow rates. Case-2 follows a similar trend, with values increasing from 45.2 W/m²·K to 54.9 W/m²·K. In Case-3, the coefficient starts at 29.2 W/m²·K and reaches 45.2 W/m²·K at the highest velocity, as shown in Figure 7. Each curve reflects the average of three trials, with error bars (± values) added to indicate measurement uncertainty in h, which did not exceed 3% across the velocity range.

Cases 4 and 5 also show clear improvements. Case-4 sees an increase from 31.9 W/m²·K to 49.4 W/m²·K, while Case-5 starts at 35.4 W/m²·K and also peaks at 49.4 W/m²·K. These results reinforce the positive correlation between flow velocity and heat transfer efficiency across varying experimental conditions.

4.1.5. 30W

The experimentally determined Hc (in W/m²·K) for each of the five scenarios, which were tested throughout a velocity range of 1 to 5 m/s, are shown in Figure 8. It is evident that increased flow speed leads to better thermal performance in Case 1, as h steadily rises from 57.6 W/m²·K at the lowest velocity to 65.0 W/m²·K at 5 m/s. While the pattern is consistent with Case 1, the absolute coefficients are still relatively lower in Case 2, which exhibits a similar upward trend with values increasing from 41.1 W/m²·K to 46.0 W/m²·K.

During the same velocity span in Case 3, the Hc increases from 30.0 W/m²·K to 42.2 W/m²·K. The trend once again demonstrates the beneficial effect of velocity on convective heat transfer, even though the initial values are on the lower end. This behavior is mirrored in Case 4, when h increases from 32.9 W/m²·K to 46.0 W/m²·K. A comparable, if more modest, improvement is shown in Case 5, going from 34.3 W/m²·K at 1 m/s to 41.0 W/m²·K at 5 m/s.

The statistics consistently show that increasing flow velocity improves the convective Hc in each of the five cases. The level of improvement, however, differs depending on the particular experimental circumstances in each instance.

4.2. Comparison Re Vs Tb

4.2.1. 10W

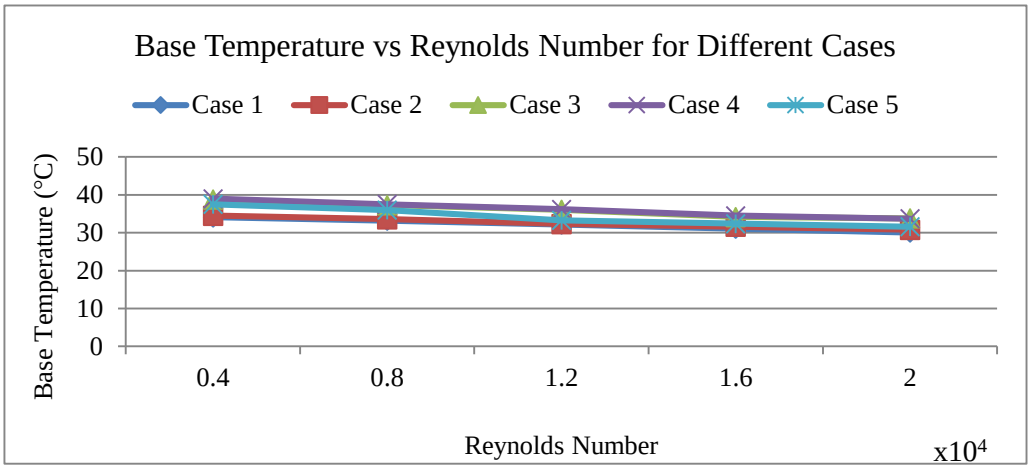

Fig. 9 10W comparative analysis of Re vs Tb, across five cases

Figure 9 presents the experimental relationship between Re and the corresponding Tb (in °C) across five distinct cases, each representing different operating conditions. Base temperature readings were averaged across three experimental runs, with observed variation remaining within ±2 °C, confirming repeatability of the results. In all cases, the Re range consistently from 4061 to 20,304. Notably, a clear inverse trend is observed between Re and Tb—higher Re correlates with lower base temperatures, indicating improved convective cooling.

In Case 1, the base temperature starts at 34.0°C at a Re of 4061 and gradually decreases to 30.0°C at 20,304. Case 2 mirrors this trend but records slightly higher temperatures throughout, beginning at 34.5°C and declining to 30.7°C. This consistent pattern continues in Cases 3, 4, and 5, with each subsequent case exhibiting marginally higher base temperatures at corresponding Re compared to the preceding one. Despite these differences in absolute temperature values, all five cases demonstrate the same fundamental behaviour: as the Re increases, the Tb decreases, highlighting the enhanced heat transfer performance at higher flow regimes.

4.2.2. 20W

Figure 10 presents experimental data illustrating the relationship between Re and the corresponding base temperatures (Tb, in °C) across five different cases, each reflecting distinct test conditions. Base temperature readings were averaged across three experimental runs, with observed variation remaining within ±2 °C, confirming repeatability of the results. The range spans from 4089 to 22,923, while the base temperatures vary within each case. In Case 1, a Re of 4089 corresponds to a base temperature of 45.0°C. As the Re increases progressively to 9007, 13,608, 18,222, and ultimately 22,923, the base temperature exhibits a gradual decline, reflecting a clear inverse relationship between flow intensity and surface temperature. This negative correlation suggests enhanced convective cooling at higher Re.

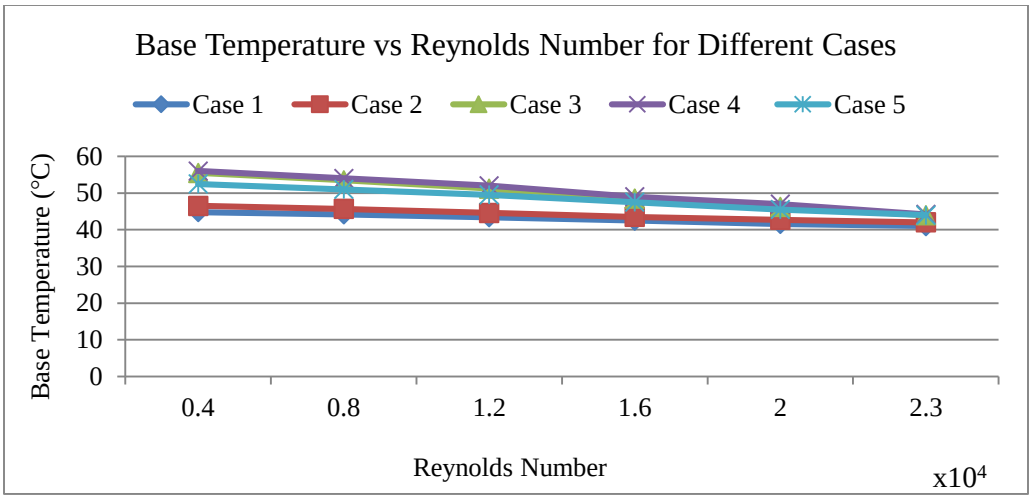

Fig. 10 20w comparative analysis of Re vs Tb across five cases

Cases 2 through 5 follow a similar trend. Case 2's base temperature decreases from 46.5°C to 41.0°C across the same Re range. Case 3 starts at 55.5°C and drops to 44.7°C, while the subsequent cases demonstrate comparable behaviour with varying initial and final temperatures. Despite differences in absolute values, the consistent downward trend in base temperature with increasing Re across all five cases highlights the beneficial impact of higher flow rates on heat dissipation efficiency.

4.2.3. 30W

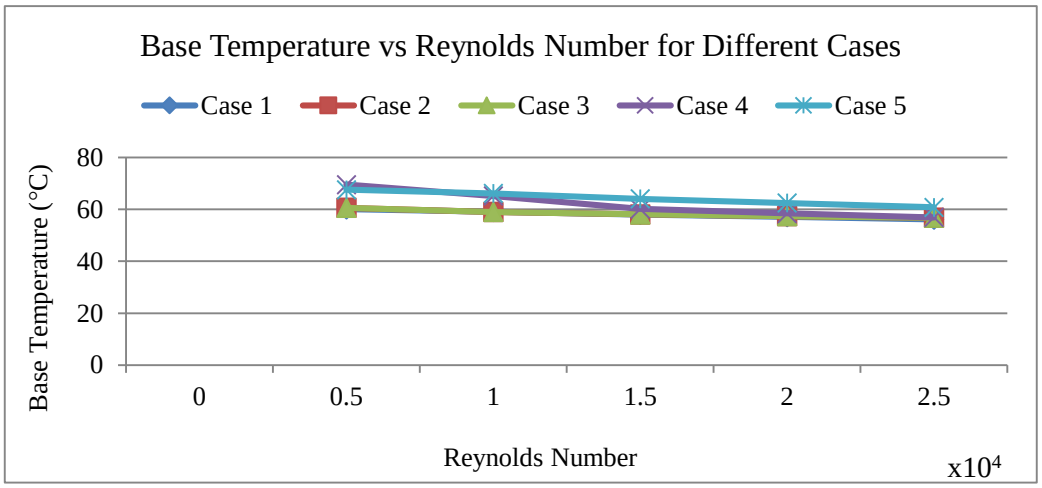

Fig. 11 30w comparative analysis of Re vs Tb across five cases

The data present the Re and corresponding Tb for five experimental cases evaluated under varying flow conditions. For every case, both Re numbers and base temperatures are recorded across multiple experimental runs to assess thermal behaviour under different regimes. In Case 1, the Re begins at 4118, corresponding to a Tb of 60.0°C, with subsequent readings showing a gradual decline in temperature as the Re increases—indicating a typical inverse relationship often observed in convective heat transfer scenarios. However, this trend is not universally consistent across all cases.

In Case 2, the base temperature is 59.0°C at Re = 9989, then increases gradually to 66.2°C at higher Re. Cases 3–5 present similar mixed patterns where Re, for example, 15200 and 20448, have based temperatures that change slightly, rising or falling, depending on the flow and thermal parameters.

In general, although some cases support a negative correlation between Re and base temperature, there are cases with a positive correlation or with non-linear correlation, which implies that the effect of Re on base temperature might depend on other parameters, including thermal boundary conditions, fluid properties or surface properties. This subtle behaviour emphasizes the intricate coupling between flow and heat transfer in realistic experiments.

4.2.4. Discussions

The thermal performance of five different heat sink designs was tested at three different power dissipation values (10W, 20W, and 30W) with four air-side heat transfer parameters: 7c, N, Hct and Tb. Analyzing the monitored data provides useful trends and comparisons of the performance of each design over multiple thermal and flow conditions.

4.2.5. Re vs Nu

At each power level, a similar apparent effect was observed, as would be expected; higher Re, and hence flow rates, were associated with higher Nu (a measure of convective heat transfer). This correlation supports the hypothesis that the more fluid motion allowed, the more efficient the thermal energy dissipation from the heat sink surface.

At 10W, Case-1 (PFHS) and Case-5 (probably PCMPFHS or another advanced design) were options. (the solid and dashed lines represented case-2) by which the Nu increased monotonically from 285 to 513, implying excellent heat transfer efficiency in convection. Case-5, on the other hand, achieved the highest Nu values throughout the increasing Re range, even though its initial Nu was lower than that of some cases, which illustrates better design or material qualities.

At 20W, Case-1 again exhibited dominant thermal behaviour, with Nu ranging from 2577 to 3211. Case-5 also maintained a commendable performance with values climbing from 811 to 1130, reinforcing the earlier trend. Case-4 consistently underperformed across all Re, indicating potential geometric or material limitations that inhibit turbulent or efficient heat exchange.

At 30W, the pattern persisted with Case-1 achieving the highest Nu (up to 2202), followed by Case-3 and Case-5. The consistent positive correlation across all cases reaffirms that enhanced flow dynamics directly improve heat dissipation capabilities. Interestingly, despite the power increase, Case-2 continued to exhibit relatively lower Nu values, highlighting design limitations in convective transfer scalability.

4.2.6. Hc vs Velocity

Velocity plays a vital role in determining the Hc, and the results reinforce this principle. A clear and consistent increase in h with rising velocity was observed across all power levels and cases, confirming the beneficial impact of higher fluid velocity on convective thermal performance.

At 10W, Case-1 again showcased the highest values (74.8 to 134.4 W/m²·K), followed by Case-2 and Case-5. Cases 3 and 4, while showing improvements with velocity, lagged in absolute performance. At 20W, the pattern was consistent but with a narrower performance gap among the configurations. Case-1 led with values from 67.2 to 84.0 W/m²·K, while other cases followed with lower yet positively trending values.

At 30W, all cases exhibited rising h with velocity, but overall gains were less pronounced, especially for Cases 4 and 5. This higher-power plateau effect may indicate thermal saturation or limitations in surface area utilization under increased thermal loads, especially for lower-performing geometries.

4.2.7. Re vs Tb

The inverse relationship between Re and Tb is evident at 10W and 20W, indicating that higher flow rates can enhance cooling and reduce thermal stagnation at the heat sink's base.

At 10W, all cases displayed this anticipated trend with the base temperature steadily decreasing as Re was increased. Case 1 showed the minimal base temperatures over the entire range of Re, indicating its better thermal management characteristic.

At 20 W, the trend is also reversed, but the spread of the upper and lower performing cases was relatively higher than the other cases because thermal loading becomes dominant. Case-3 began at a much higher initial base temperature (55.5°C), highlighting its weakness under low heating loads.

Nevertheless, at 30W, alterations from the normal sequence occurred. However, as opposed to Case-1, Case-2 showed a positive correlation between Re and base temperature, indicative of possible flow channelling losses or thermal surfeit due to configuration defects. Cases 3-5 showed non-linear (non-vortex shedding) behaviors, likely implying complex interactions of flow (turbulence) with disrupted boundary layers and material (thermal conductivity) at higher heat inputs. Such factors highlight the significance of assessing heat sink performance based on geometry optimization and the thermal response of the material under higher stress, rather than only focusing on flow rate control.

4.2.8. Overall Comparative Evaluation

Case-1 (PFHS) was also the most effective among the others at all power levels and for all the metrics, and was the most effective configuration in terms of convective heat transfer and base temperature stabilization.

Even though process-5 started from lower values than process-2, thermal enhancement could be raised when the flow rate was high, suggesting its performance could be scaled to the forced convection level.

From Table 1, it was found that Case-2 and Case-4 had lower time lags, especially at high load, which might indicate that the geometry of the design had some

bottlenecks, such as the exposure of surface area was not enough or the fin/channel design was not perfect.

At 30 W, the performance separation was clearly displayed, therefore suggesting an effective heat-sinking design for high-power applications.

5. Conclusion

This study evaluated the thermal performance of five distinct heat sink configurations—PFHS, CPFHS, PPFHS, PCMPFHS, and PPFHS—under three levels of power dissipation (10W, 20W, and 30W). Previous work usually only considered geometry or materials separately, whereas in this paper, five different heat sink designs are tested under the same test conditions, and an optimization model is proposed that also includes manufacturability and cost. The analysis was carried out using key parameters including Re, Nu, Hc, and Tb. Based on the experimental results and comparative analysis, the following conclusions can be drawn:

- Heat Sink Geometry and Design Significantly Influence Thermal Performance: Among all configurations, Case-1 (PFHS) consistently demonstrated the best performance across all metrics—exhibiting the highest Nu and Hc, along with the lowest base temperatures at increasing Re and velocities. This suggests that its geometric or material design offers the most efficient convective cooling.
- Increased Flow Rate Enhances Convective Heat Transfer: Across all cases and power levels, a positive correlation was observed between Re and Nu and between fluid velocity and Hc. This confirms the fundamental principle that higher flow rates enhance convective heat transfer by reducing the thermal boundary layer.
- Higher Re Reduce Base Temperatures: For 10W and 20W conditions, all configurations exhibited a clear inverse relationship between Re and Tb, indicating improved heat dissipation with increased fluid motion. On the other hand, at 30 W, deviations occurred in certain designs (particularly Case-2), indicating a reduction in scaling efficiency and justifying further geometry optimization cases under higher thermal loads.
- Design Limitations Become Apparent at Higher Power Levels: At 30W, thermal performance gaps widened. Some heat sinks showed non-linear or inconsistent thermal behavior, highlighting the need for robust design under elevated thermal stress. These findings emphasize the importance of advanced material selection and structural optimization for high-power applications. The results provide engineers with clear guidelines to optimize the trade-offs between cooling effectiveness, material choice and cost for heat sinks in small high-power electronics.

Case-5 exhibited good positive trends with Re and velocity, which indicated that a strong scalability for forced convection (although not always better than Case-1). The results taken together affirm that pin-fin configurations, particularly perforated and PCM-enhanced designs, are promising candidates for advanced cooling systems of electronics.

5.1. Data Availability Statement

The data used and/or analysed during the current study are available from the corresponding author on reasonable request.

References

[1] Ashish Dixit, Rajesh Maithani, and Sachin Sharma, "Enhancing Electronic System Cooling: Exploring Minichannel Heat Sink Solutions," *Journal of Thermal Analysis and Calorimetry*, vol. 150, pp. 5357-5407, 2025. [CrossRef] [Google Scholar] [Publisher Link]

[2] Rilwan Kayode Apalowo et al., "Investigating the Impacts of Heat Sink Design Parameters on Heat Dissipation Performance of Semiconductor Packages," *International Journal of Thermal Sciences*, vol. 208, 2025. [CrossRef] [Google Scholar] [Publisher Link]

[3] Xiong Zhao et al., "Microfluidic One-Step and Large-Scale Production of Silica and Titania Nanofluids toward Phase-Change Heat Transfer Intensification of Power Electronic Devices," *Chemical Engineering Journal*, vol. 503, 2025. [CrossRef] [Google Scholar] [Publisher Link]

[4] Hussam Sadique, Qasim Murtaza, and Samsher, "Heat Transfer Augmentation in Microchannel Heat Sink Using Secondary Flows: A Review," *International Journal of Heat and Mass Transfer*, vol. 194, 2022. [CrossRef] [Google Scholar] [Publisher Link]

[5] Qinghua Wang et al., "Numerical Simulation of Fluid and Heat Transfer Characteristics of Microchannel Heat Sink with Fan-Shaped Grooves and Triangular Truncated Ribs," *International Communications in Heat and Mass Transfer*, vol. 155, 2024. [CrossRef] [Google Scholar] [Publisher Link]

[6] Rimpy Singh, "Numerical Simulation and Optimization of Fin Configurations for Enhanced Heat Sink Performance in Aluminum and Copper Materials," *Mechanical and Aerospace Engineering Theses*, pp. 1-57, 2024. [Google Scholar] [Publisher Link]

[7] S.R. Akhil Krishnan et al., "Experimental and Numerical Investigation on the Performance of Binary Solid-Solid Phase Change Materials with Integrated Heat Pipe and Aluminium Foam Based Heat Sink for Thermal Management of Electronic Systems," *International Journal of Thermal Sciences*, vol. 208, 2025. [CrossRef] [Google Scholar] [Publisher Link]

[8] C.M. Ramesha et al., "Enhancing Thermal Conductivity of Aluminium 6063 Alloy by Adding Titanium for Advanced Heat Sink Applications," *Innovations in Electronic Materials: Advancing Technology for a Sustainable Future*, pp. 377-384, 2025. [CrossRef] [Google Scholar] [Publisher Link]

[9] Ahmad Ali Awais, and Man-Hoe Kim, "Experimental and Numerical Study on the Performance of a Minichannel Heat Sink with Different Header Geometries Using Nanofluids," *Applied Thermal Engineering*, vol. 171, 2020. [CrossRef] [Google Scholar] [Publisher Link]

[10] Zannatul Mehjabeen et al., "Numerical Study of Arrowhead, Hexagonal, and Concave Shaped-Elliptical Perforated Plate Fin Heatsinks to Improve the Hydrothermal Performance Factor," *International Journal of Thermal Sciences*, vol. 207, 2025. [CrossRef] [Google Scholar] [Publisher Link]

[11] Ayushman Srivastav, Rajesh Maithani, and Sachin Sharma, "Innovative Impinging Jet Methods for Performance Enhancement: A Review," *Journal of Thermal Analysis and Calorimetry*, vol. 149, pp. 13581-13627, 2024. [CrossRef] [Google Scholar] [Publisher Link]

[12] Mohammad Harris et al., "Heat Transfer Optimisation using Novel Biomorphic Pin-Fin Heat Sinks: An Integrated Approach via Design for Manufacturing, Numerical Simulation, and Machine Learning," *Thermal Science and Engineering Progress*, vol. 51, 2024. [CrossRef] [Google Scholar] [Publisher Link]

[13] Tao Yang et al., "A Review on Application of Pin-Fins in Enhancing Heat Transfer," *Energies*, vol. 17, no. 17, pp. 1-17, 2024. [Google Scholar] [Publisher Link]

[14] Jie Li et al., "Thermal Performance of Pin Fin Heat Sinks with Phase Change Material for Electronic Devices Thermal Management," *Applied Thermal Engineering*, vol. 250, 2024. [CrossRef] [Google Scholar] [Publisher Link]

[15] Naushad Ali et al., "Heat Dissipation and Fluid Flow in Micro-Channel Heat Sink Equipped with Semi-Elliptical Pin-Fin Structures: A Numerical Study," *International Communications in Heat and Mass Transfer*, vol. 155, 2024. [CrossRef] [Google Scholar] [Publisher Link]

[16] F.L. Tan, and C.P. Tso, "Cooling of Mobile Electronic Devices Using Phase Change Materials," *Applied Thermal Engineering*, vol. 24, no. 2-3, pp. 159-169, 2004. [CrossRef] [Google Scholar] [Publisher Link]

[17] Dhamyaa S. Khudhur, Reyadh Ch Al-Zuhairy, and Muna S. Kassim, "Thermal Analysis of Heat Transfer with Different Fin Geometry through Straight Plate-Fin Heat Sinks," *International Journal of Thermal Sciences*, vol. 174, 2022. [CrossRef] [Google Scholar] [Publisher Link]

[18] V.C. Midhun, Mayank Maroliya, and Sandip K. Saha, "Numerical Investigation and Optimisation of Solid–Solid Phase Change Material Composite-Based Plate-Fin Heat Sink for Thermal Management of Electronic Package," *Applied Thermal Engineering*, vol. 248, 2024. [CrossRef] [Google Scholar] [Publisher Link]

[19] Ozgun Kosdere, Zerrin Sert, and Ozge Altun, "Investigation of Thermal Performance at Forced Convection in Plate-Fin Heat Sink," *Energy*, vol. 307, 2024. [CrossRef] [Google Scholar] [Publisher Link]

[20] Kitti Nilpueng, Preecha Kaseethong, and Somchai Wongwises, "Heat Transfer and Flow Characteristics of a Plate-Fin Heat Sink Equipped with Copper Foam and Twisted Tapes," *Heliyon*, vol. 10, no. 12, pp. 1-12, 2024. [CrossRef] [Google Scholar] [Publisher Link]

[21] Athasit Wongcharoen et al., "Influence of Pin-Perforation Shape on Thermohydraulic Performance of Circular Pin-Fin Heat Sinks under Turbulent Flow," *Ain Shams Engineering Journal*, vol. 15, no. 5, pp. 1-12, 2024. [CrossRef] [Google Scholar] [Publisher Link]

[22] Yousef Alihosseini et al., "Oblique Microchannel Merged with Circle Micro Pin-Fin as a Novel Hybrid Heat Sink for Cooling of Electronic Devices," *Case Studies in Thermal Engineering*, vol. 53, pp. 1-15, 2024. [CrossRef] [Google Scholar] [Publisher Link]

[23] Zahid Maqbool, M. Hanief, and Malik Parveez, "Review on Performance Enhancement of Phase Change Material Based Heat Sinks in Conjugation with Thermal Conductivity Enhancers for Electronic Cooling," *Journal of Energy Storage*, vol. 60, 2023. [CrossRef] [Google Scholar] [Publisher Link]

[24] Imran Zahid et al., "Experimental Optimization of Various Heat Sinks Using Passive Thermal Management System," *Case Studies in Thermal Engineering*, vol. 49, pp. 1-13, 2023. [CrossRef] [Google Scholar] [Publisher Link]

[25] Tauseef-ur Rehman, and Cheol Woo Park, "Optimising Heat Sink Performance with Porous Media–PCM Integration: An Experimental Investigation," *Applied Thermal Engineering*, vol. 242, 2024. [CrossRef] [Google Scholar] [Publisher Link]

[26] Deepa Gupta, Probir Saha, and Somnath Roy, "Computational Analysis of Perforation Effect on the Thermo-Hydraulic Performance of Micro Pin-Fin Heat Sink," *International Journal of Thermal Sciences*, vol. 163, 2021. [CrossRef] [Google Scholar] [Publisher Link]

[27] Muhammad Anas Wazir et al., "Thermal Enhancement of Microchannel Heat Sink Using Pin-Fin Configurations and Geometric Optimization," *Engineering Research Express*, vol. 6, no. 1, pp. 1-25, 2024. [CrossRef] [Google Scholar] [Publisher Link]

[28] Taha Tuna Göksu, "Investigation of Pin and Perforated Heatsink Cooling Efficiency and Temperature Distribution," *Journal of Thermal Analysis and Calorimetry*, vol. 149, no. 12, pp. 6517-6529, 2024. [CrossRef] [Google Scholar] [Publisher Link]

[29] Behzad Heidarshenas et al., "Numerical Study and Optimization of Thermal Efficiency for a Pin Fin Heatsink with Nanofluid Flow by Modifying Heatsink Geometry," *Case Studies in Thermal Engineering*, vol. 55, pp. 1-18, 2024. [CrossRef] [Google Scholar] [Publisher Link]

[30] Ahmed Dhafer Abdulsahib, Dhirgham Alkhafaji, and Ibrahim M. Albayati, "Thermal Design and Heat Transfer Analysis of Heat Sinks and Enclosures: A Review," *International Journal of Heat and Technology*, vol. 42, no. 4, pp. 1149-1163, 2024. [CrossRef] [Google Scholar] [Publisher Link]

[31] Xiaoling Yu et al., "Development of a Plate-Pin Fin Heat Sink and Its Performance Comparisons with a Plate Fin Heat Sink," *Applied Thermal Engineering*, vol. 25, no. 2-3, pp. 173-182, 2005. [CrossRef] [Google Scholar] [Publisher Link]

[32] H. Shaukatullah et al., "Design and Optimization of Pin Fin Heat Sinks for Low Velocity Applications," *IEEE Transactions on Components, Packaging, and Manufacturing Technology: Part A*, vol. 19, no. 4, pp. 486-494, 1996. [CrossRef] [Google Scholar] [Publisher Link]

[33] Maissa Bouguila et al., "Thermal Performances of Finned Heat Sink Filled with Nano-Enhanced Phase Change Materials: Design Optimization and Parametric Study," *International Journal of Heat and Mass Transfer*, vol. 202, 2023. [CrossRef] [Google Scholar] [Publisher Link]

[34] Ahmed Abdulnabi Imran, Nabeel Sameer Mahmoud, and Hayder Mohammad Jaffal, "Numerical and Experimental Investigation of Heat Transfer in Liquid Cooling Serpentine Mini-Channel Heat Sink with Different New Configuration Models," *Thermal Science and Engineering Progress*, vol. 6, pp. 128-139, 2018. [CrossRef] [Google Scholar] [Publisher Link]

[35] Rajesh Baby, and C. Balaji, "Thermal Performance of a PCM Heat Sink under Different Heat Loads: An Experimental Study," *International Journal of Thermal Sciences*, vol. 79, pp. 240-249, 2014. [CrossRef] [Google Scholar] [Publisher Link]

[36] Haluk Anil Kose, Alperen Yildizeli, and Sertac Cadirci, "Parametric Study and Optimization of Microchannel Heat Sinks with Various Shapes," *Applied Thermal Engineering*, vol. 211, 2022. [CrossRef] [Google Scholar] [Publisher Link]

[37] K. Shailesh, Y. Naresh, and J. Banerjee, "Heat Transfer Performance of a Novel PCM Based Heat Sink Coupled with Heat Pipe: An Experimental Study," *Applied Thermal Engineering*, vol. 229, 2023. [CrossRef] [Google Scholar] [Publisher Link]

[38] R. Srikanth, and C. Balaji, "Experimental Investigation on the Heat Transfer Performance of a PCM Based Pin Fin Heat Sink with Discrete Heating," *International Journal of Thermal Sciences*, vol. 111, pp. 188-203, 2017. [CrossRef] [Google Scholar] [Publisher Link]

[39] Reiyu Chein, and Jason Chuang, "Experimental Microchannel Heat Sink Performance Studies Using Nanofluids," *International Journal of Thermal Sciences*, vol. 46, no. 1, pp. 57-66, 2007. [CrossRef] [Google Scholar] [Publisher Link]